Polymer light-emitting field-effect transistors with hole mobility exceeding 1 cm^2 V^{-1} s^{-1}

Mujeeb Ullah Chaudhry[*1], *Julianna Panidi*[2], *Sungho Nam*[3], *Alice Smith*[3], *Jongchul Lim*[3], *Kornelius Tezner*[2], *Panos A. Patsalas*[4], *George Vourlias*[4], *Wai-Yu Sit*[2], *Yuliar Firdaus*[5], *Martin H. Heeney*[6], *Donal D. C. Bradley*[*3,7], *Thomas D. Anthopoulos*[*2,5]

[1] Department of Engineering, Durham University, Durham, DH1 3LE, United Kingdom
[2] Blackett Laboratory, Department of Physics & Centre for Plastic Electronics, Imperial College London, London SW7 2BW, United Kingdom
[3] Department of Physics, University of Oxford, Oxford OX1 3PU, United Kingdom
[4] Department of Physics, Laboratory of Applied Physics Aristotle University of Thessaloniki, GR-54124, Greece
[5] Physical Science and Engineering Division, King Abdullah University of Science and Technology (KAUST), KAUST Solar Centre, Thuwal 23955, Saudi Arabia
[6] Department of Chemistry & Centre for Plastic Electronics, Imperial College London, London SW7 2BW, United Kingdom
[7] Department of Engineering Science, University of Oxford, Oxford OX1 3PJ, United Kingdom

* Correspondence: mujeeb.u.chaudhry@durham.ac.uk (MUC), donal.bradley@mpls.ox.ac.uk (DDCB), thomas.anthopoulos@kaust.edu.sa (TDA)

Abstract

The vast majority of conjugated polymer-based light emitting field-effect transistors (LEFETs) are characterized by low charge carrier mobilities typically in the range 10^{-5} to 10^{-3} cm^2 V^{-1} s^{-1} range. Fast carrier transport is a highly desirable characteristic for high frequency LEFET operation and, potentially, for use in electrically-pumped lasers. Unfortunately, high mobility organic semiconductors are often characterised by strong intermolecular π-π interactions that reduce luminescence. Development of new materials and/or device concepts that overcome this hurdle are therefore required. We report single organic semiconductor layer, light-emitting transistors that combine the highest hole mobilities reported to date for any polymer-based LEFET, with encouraging light emission characteristics. We achieve this in a single polymer layer LEFET, which was further enhanced through the use of a small-molecule/conjugated polymer blend system that possesses a film microstructure which supports enhanced charge carrier mobility (3.2 cm^2 V^{-1} s^{-1}) and promising light emission characteristics (1600 cd m^{-2}) as compared to polymer-only based LEFETs. This simple approach represents an attractive strategy to further advance the performance of solution-processed LEFETs.

The performance of organic field effect transistors (OFETs) has been improving rapidly in recent years and charge carrier mobilities are now higher than amorphous silicon (Si) (1-4), offering performance adequate for various electronic and display applications. In addition, the versatility of organic semiconductors has allowed development of interesting bifunctional devices such as light-sensing (LSFETs) (5-6) and light-emitting (LEFETs) FETs (7-12). The demonstration of the first organic LEFETs in 2003 instigated a major research effort focused on the development of novel device architectures (13-19) and high mobility light-emitting materials (14,20) with a significant potential for a wider range of applications including, active matrix colour displays, biomedical sensors, integrated circuits and in communication devices. Furthermore, it was argued that for the development of electrically-pumped organic laser diodes, a similar materials optimisation may be required (1, 21). Unfortunately, combining high charge carrier mobility and efficient light emission in organic materials has proven challenging (21-25), because on one hand the reduction of inter-chain interactions benefits the luminescence efficiency but on the other hand it suppresses charge transport (26). Currently, best-performing solution-processed polymer LEFETs show carrier mobilities significantly lower (10^{-3} to 10^{-5} cm^2 V^{-1} s^{-1}) than small-molecule based LEFETs ($\approx$1 cm^2 V^{-1} s^{-1}) (14,15,25) but with significantly higher electroluminescence efficiencies (11,13). To address this challenge, multilayer channel LEFET architectures have also been developed (13, 18-19) with primary aim to decouple the charge transport process from light emission. Unfortunately, multilayer channels require complex processing often resulting to poor efficiencies due to imbalance charge transport. The development of novel organic semiconductor systems that combine high mobility with efficient light emission characteristics is therefore timely for the broader area of LEFETs.

Recently, high mobility OFETs have been fabricated using binary and ternary small-molecule/conjugated polymer blends (27-31). Blend OFETs combine the advantageous properties of solution processing with superior charge transport characteristics that compare favorably with the best-in-class OFETs reported to date (29,31). Motivated by the blend approach, we wondered whether carefully designed blend channels can indeed be implemented in LEFETs. To test this hypothesis we combined the high hole mobility (>20 cm^2 V^{-1} s^{-1}) (29,30), and solution processable, small-molecule 2,7-dioctyl[1]-benzothieno[3,2-b][1]benzothiophene (C$_8$-BTBT) (4), with the polymeric semiconductor poly[[6,6,12,12-tetrakis(4-hexadecylphenyl)-6,12-dihydroindeno[1,2-b]indeno[2',1':4,5]thieno[2,3-d]thiophene-2,8-diyl]thieno[3,2-b]thiophene-2,5-diyl] (PDITTTT) (35) to form the blend

channel layer. C_8-BTBT is a wide band gap material ($\approx$3.6 eV) known for its ultra-high hole mobility and non-emissive characteristics (photoluminescence quantum efficiency, PLQE, of $\approx$0.5%). Therefore, its application in LEFETs will most certainly require the presence of an emissive component that can be excited via Förster energy transfer during device operation (30-31). PDITTTT, on the other hand (35), is similar to other donor-acceptor copolymers reported previously and used extensively in organic solar cells (36). Surprisingly, we found that C_8-BTBT:PDITTTT blend LEFETs exhibit hole mobility (μ_h) of $\approx$3 cm^2 $V^{-1}s^{-1}$ -a value higher than any previously reported LEFETs (8-11)- this combined with high electroluminance (1600 cd m^{-2}) exceeds the state-of-the-art performance in solution-processed LEFETs (8-13) and even LEFETs made of organic single crystals (25). Furthermore, the top-gate architecture employed in combination with the fluoropolymer gate dielectric CYTOP^{TM}, results in LEFETs with enhanced environmental stability.

Fig. 1a shows the chemical structure of PDITTTT with its extended fused-ring sequence driving a high degree of molecular planarity. The normalised UV-Vis absorption and photoluminescence (PL) spectra of a PDITTTT thin film (534 nm, pumped at 405 nm) before and after annealing at 120 °C are shown in **Fig. 1b,** while normalised UV-Vis absorption and PL spectra of the C_8-BTBT film (367 nm, pumped at 340 nm) before and after annealing at 120 °C are shown in **Fig. S1** in Supporting Information. **Fig. 1c** & **1d** show, the molecular structure of C_8-BTBT along with the normalised UV-vis absorption and PL spectra of the C_8-BTBT:PDITTT blend film (534 nm, pumped at 405 nm) before and after annealing at 120 °C. The blend ratio was optimised in terms of transistors performance at 1:3 (by weight) of small molecule to polymer, further details on solution processing is presented in the Experimental Section. The vibronic absorption and PL of the neat PDITTTT films show that its long side chains are not adversely impacting the planarity of the molecule, nor creating high levels of disorder within the film. This structure is preserved with the addition of C_8-BTBT, however the scattering tail seen in the 'As Spun' blend film suggests a rougher surface than the neat PDITTTT film. This feature is retained post annealing, but to a much lesser degree, indicating that the thermal processing has helped to smooth the surface of the blend layer. The C_8-BTBT absorption peak at 359 nm (given in **Supporting Information, Fig. 1d** and **Fig. S1**), is clearly seen in the blend absorption, however its emission at 367 nm (**Fig. 1d** and **Fig. S1)** is not visible, due to Förster energy transfer to the PDITTTT chromophore, resulting in a PL spectrum consistent with neat the PDITTTT film (534 nm). The relatively small spectral overlap in the PL of C_8-BTBT and PDITTTT highlights the possibility of replacing PDITTTT with more

absorbing units/materials in order to improve Förster energy transfer. The PLQE of PDITTTT and blend films, pumped at 405nm, were 11.7 %, and 13.3 % respectively. The PLQE of C_8-BTBT film (pumped at 340 nm) was $\approx$ 0.5 %. The PLQE and absorption parameters for the various materials studied are provided **Fig. S2, S3** and **Table S1** in **Supporting Information**.

It is known that reducing the refractive indices of the constituent layers in an organic light emitting device can enhance light extraction (37). Lowering the refractive index of the organic layers can thus reduce light coupling to the thin-film guided modes and suppress Fresnel reflection from the boundaries (38). As determined by variable angle spectroscopic ellipsometry (VASE), the refractive index of C_8-BTBT and PDITTTT were 1.6 and 2 at 550 nm (see **Figs. S4** and **S5** in Supporting Information). The refractive index was reduced to 1.8 at 550 nm (**Fig. S6**, in **Supporting Information**) after mixing the PDITTTT with C_8-BTBT, which could result in factor of 1.2 increase of η_{out} at 550 nm from crude calculation ($\eta_{out} = 1/2n^2$, where n is the refractive index of the material in which the light is generated).

To further investigate the optical properties of thermally annealed (120 °C) PDITTTT and C_8-BTBT:PDITTTT blend films, time-resolved PL (TRPL) (pumped at 405 nm) measurements were performed (**Fig. 2a**, **Fig. S7** and **S8**). A bi-exponential decay was observed for both films with slightly longer decay times for the C_8-BTBT:PDITTTT blend ($t_1 \approx 0.090$ ns and $t_2 \approx 1.00$ ns) than for the pristine PDITTTT ($\tau_1 \approx 0.083$ and $\tau_2 \approx 0.89$). The TRPL curves for the pristine C_8-BTBT film (absorption edge $\approx$ 340 nm, $PL_{\lambda max} \approx$ 370 nm) could not be recorded due to instrument limitation.

The microstructure of PDITTTT and C_8-BTBT:PDITTTT blend films were also studied using atomic force microscopy (AFM) and X-ray diffraction (XRD) measurements (**Fig. 2b, 2c** and **2d**). From the AFM images we observe that the PDITTTT films appear smooth and largely disordered with no evidence of strong surface features (**Fig. 2b** and **Fig. S9**). Blend films, on the other hand, appear polycrystalline (**Fig. 2c**). The polycrystalline nature of the blend film is attributed to the phase separation of C_8-BTBT to the surface of the blend film and the formation of large polycrystalline domains in the top layers, in accordance with previous results (26-29). XRD measurements were obtained in the Bragg-Brentano geometry for C_8-BTBT, PDITTTT and C_8-BTBT:PDITTTT blend films (**Figure 2d**). The PDITTTT film was found to be amorphous without noticeable diffraction peaks. Conversely, C_8-BTBT and C_8-

BTBT:PDITTTT blend samples exhibit diffraction patterns that are broadly consistent with the C_8-BTBT powder diffractogram (39). For C_8-BTBT, the stronger diffraction peaks are observed at around 6° and 9° and correspond to (00h) planes, which is typical for the formation of rod-like crystals. In the case of the blend film, the (020) peak also emerges, which is usually a manifestation of strain (40). This suggestion is supported by the evident shift of the (002) peak upon blending (see inset in **Fig. 2d**) which confirms a substantial deformation of the C_8-BTBT crystal cell. In addition, the shift is accompanied by changes in the profile of this peak, namely a reduced intensity and increased broadening. The calculated values of microstrain, as extracted by fitting the three prominent (002) diffraction peaks to Voigt curves (with both Lorentzian and Gaussian contributions) were exceptionally small and similar across both samples. This suggests that the deformation of the C_8-BTBT within the blend is of a hydrostatic nature and does not cause any additional structural defects, which were assigned to reduced lateral size of organic molecule lamellae in contrast to the case of dif-TES-ADT as previously reported (4). Finally, the vertical grain size (G_z) was calculated to be ≈69 nm for C_8-BTBT *versus* ≈38 nm for the binary blend. As the lateral lamellar size is not affected by blending, it seems that the polymer is distributed in between of the wide C_8-BTBT lamellae along the z-direction resembling an intercalation process.

The electrical properties of the polymer and blend films were evaluated using bottom-contact, top-gate (BC-TG) FETs (**Fig. 3**). Gold source-drain (S-D) electrodes were treated with the self-assembled monolayer (SAM) 2,3,4,5,6-Pentafluorothiophenol (PFBT) to improve hole injection (41). The organic semiconducting materials and the dielectric layer were then deposited via spin coating followed by thermal annealing at 120 °C in a nitrogen filled glovebox. The device fabrication was completed with the deposition of Al gate electrodes. Further details of material preparation and fabrication methods can be found in the ***Materials and Methods*** section.

A representative set of PDITTTT transistor transfer characteristics (channel length (L) and width (W) of 50 and 1000 μm) is shown in **Fig. 3b**. The devices exhibit excellent hysteresis-free *p*-channel operation in both linear (V_{DS} = - 20 V) and saturation (V_{DS} = - 100 V) regimes with channel current ON/OFF ratio >10^5. The electrical output characteristics for this particular device are shown in **Fig. 3c**, with saturation regime hole mobility $\mu_{h,sat} \approx 1$ cm^2 V^{-1} s^{-1}. A similar device architecture was used to fabricate the C_8-BTBT:PDITTTT blend transistors (**Fig. 3**) and the corresponding transfer and output characteristics are shown in **Fig.**

3d and **3e**. In the blend films an emergence of the small and insignificant hysteresis is observed, with a substantially lower ON/OFF ratio ($>10^3$) than for the PDITTTT-only devices, this might be due to increased conducting paths in blend films and rougher films. However, saturation regime hole mobility $\mu_{h,sat} \approx 1.6$ cm^2 V^{-1} s^{-1} is slightly higher. To exclude any overestimation in the FET mobility calculations (42-43), we further analysed the calculated mobility values following the method proposed by Choi *et al.* (43) (see **Supplementary Information**). The associated reliability factor was calculated and used to determine FET ideality-corrected effective mobilities for both devices, yielding $\mu_{h,eff} \approx 0.63$ and 0.83 cm^2 V^{-1} s^{-1} for polymer and blend FETs, respectively (**Table S2** in **Supplementary Information**).

In a similar manner, polymer and blend LEFETs were fabricated in BC-TG architecture (**Fig. 4a**) but this time using asymmetric S-D electrodes. PFBT-functionalised Au was used as hole injecting electrode, whilst a combination of caesium carbonate/silver (Cs$_2$CO$_3$/Ag) was used for electron injection. The pristine PDITTTT LEFETs exhibited strictly unipolar *p*-channel behaviour with a current ON/OFF ratio of $>10^5$ (**Fig. 4b**) and $\mu_{h,sat} \approx 0.8$ cm^2 V^{-1} s^{-1}. Despite the absence of clear electron accumulation within the channel, electron injection from the Cs$_2$CO$_3$/Ag electrode into the lowest unoccupied molecular orbital (LUMO) energy state of PDITTTT (-3 eV) does take place as evident by the light emission occurring in close proximity to the electron injecting electrode. However, we determined electron mobilities in *space charge limited current* scenario in a diode configuration of glass/Al/Cs$_2$CO$_3$/(polymer or blend)/Cs$_2$CO$_3$/Al) which were $\approx 5.6 \times 10^{-8}$ cm^2 V^{-1} s^{-1} and 6×10^{-8} cm^2 V^{-1} s^{-1} for PDITTTT and C8:BTBT:PDITTTT films, respectively (**Fig. S10**). The corresponding output characteristics are shown in **Fig. 4d** and **4e**. Similarly, *p*-channel dominated operation was observed for the C$_8$-BTBT:PDITTTT blend transistors (**Fig. 4c**) but with a significantly higher $\mu_{h,sat}$ (7 cm^2 V^{-1} s^{-1}) and a lower current ON/OFF ratio ($\approx 10^3$). The output characteristics of a representative blend LEFET are shown in **Fig. 4f**. Finally, the transistors' mobility reliability factors were also calculated yielding values for $\mu_{h,eff}$ of 0.42 and 3.2 cm^2 V^{-1} s^{-1} for the pristine PDITTTT and C$_8$-BTBT:PDITTTT based devices, respectively (**Supplementary Information, Table S1**).

Fig. 5a and **5b** show, respectively, the luminance, L, (cd/m^2) and external quantum efficiency, EQE (%), for PDITTTT LEFETs as a function of gate-source voltage (V$_{GS}$). In the case of top emission, L increases for $|V_{GS}| > -18$V and reaches ≈ 100 cd m^{-2} at V$_{GS}$ = -150 V, with an EQE of $\approx 1.3 \times 10^{-2}$ %. For bottom emission, L ≈ 300 cd m^{-2} at V$_{GS}$ = -150 V, with the

EQE = 3.1×10^{-2} %. The improved performance in bottom-emission is mainly due to higher transmittance (~89%, see **Fig. S11**), as compared to the reflective semi-transparent Al gate electrode (~20%). **Fig. 5c** and **5d** show the corresponding L and EQE characteristics for the C_8-BTBT:PDITTTT blend LEFETs where L $\approx$ 500 cd m^{-2} (EQE = 1×10^{-2} %) measured for top emission and L $\approx$ 1700 cd m^{-2} (EQE = 4×10^{-2} %) measured for bottom emission at V_{GS} = -150 V. Therefore, blend LEFETs clearly show enhanced light-emission than pristine polymer LEFETs in addition to their enhanced electrical performance. Finally, the maximum current densities (hole) passing through the recombination zone for polymer only and blend devices were calculated to be 1.6 A/cm^2 and 3.6 A/cm^2, respectively (**Fig. S12** and **S13**). These results are summarized in **Table 1** together with a performance comparison against previously reported polymer LEFETs found in the literature. Although the improved performance in our LEFETs arises from extended fused-ring sequence in PDITTTT molecules providing a high degree of planarity and order within the films, and the long side chains provide spacing to prevent quenching of photoluminescence, while these features are preserved in neat and blend film. However, on the basis of these results we conclude that the limiting factor for efficient light emission in this type of LEFETs is the transport of electrons, which is subject of ongoing research in material development. Simultaneous improvement of electron injection and ambipolar charge transport is essential for realising ideal LEFETs.

Fig. 5e shows optical images of two LEFETs based on the pristine polymer and blend during operation. The emission area appears as a narrow zone in close proximity to the electron injecting Cs_2CO_3/Ag electrode, which is indicative of the highly imbalanced charge transport discussed above. The width of emission zone was estimated at around $\approx$6 μm for polymer only LEFET and $\approx$14 μm for blend LEFET (see **Fig. S14** and **Fig S15** in **Supporting Information**). The broader emission pattern seen in the blend LEFET may well be attributed to the non-uniform and highly texture surface of the blend channel rather than being an intrinsic device property. Moreover, the electroluminescence (EL) spectrum for a pristine polymer and a blend LEFET measured from the top, are shown as black lines in **Fig. 5f** and **Fig. 5g**, respectively. Both emission spectra appear identical with the characteristic vibronic features largely matching those seen in the corresponding PL spectra (blue lines).

The operation of these LEFETs can be understood by considering the energy levels of the materials used to construct them (**Fig. S16**). Negative V_{GS} (< 0 V) and V_{DS} (< 0 V) helps to

inject and accumulate holes at the polymer / CYTOP or blend / CYTOP interface. The mobile holes move across the LEFET channel and recombine with injected electrons in close proximity to the drain electrode (i.e. Cs_2CO_3 / Ag) as evident by the microscope images shown in **Fig. 5e**. The internal quantum efficiency or otherwise known as recombination efficiency was also calculated using the measured photoluminescence quantum yield (PLQE) values for the pristine polymer ($\approx$11.7 %) and blend ($\approx$13.3 %) films, yielding modest values of 5.8 % and 5.1 %, respectively, measured at the highest operating voltages. Importantly, the use of CYTOP appears to be highly advantageous in terms of environmental stability of the LEFETs since all devices could be stored in ambient air for over 4 weeks before small performance degradation was observed ($\approx$3%, shown in **Fig. S17**).

In summary, we have demonstrated PDITTTT polymer and binary C_8-BTBT: PDITTTT blend based transistors and light-emitting transistors with maximum hole mobility values (3.2 $cm^2V^{-1}s^{-1}$) significantly higher than any previously reported polymer-based LEFETs. Carefully engineered devices exhibit green light emission with modest brightness levels (1600 cd/m^2) and an internal quantum efficiency of ~ 5 %. Importantly, the top-gate LEFETs exhibit long shelf lifetimes, a characteristic attributed to the use of CYTOP as the gate dielectric. These results present a significant step towards LEFETs that combine high carrier mobility with appreciable light emitting characteristics, hence making small molecule/polymer blends an attractive option for numerous opto-electronic applications.

Materials and Methods

Solution preparation: Conjugated polymer PDITTTT (35), containing diindeno-thieno [3,2-b]thiophene based polycyclic repeat units with a MW of 242k and a polydispersity of 2.85 as measured by GPC against polystyrene standards, was obtained from Merck GMBH. A solution of 10 mg mL^{-1} of PDITTT was prepared using anhydrous 1,2,3,4-tetrahydronaphthalene (purchased by Sigma-Aldrich) and 10 mg mL^{-1} C_8-BTBT (purchased by One-Material) in anhydrous chlorobenzene where spin coated at 2000 rpm for 30 seconds. For the C_8-BTBT:PDITTTT blend formulations, 20 mg mL^{-1} solutions of the small molecule in chlorobenzene were mixed in a 1:3 ratio with 15 mg mL^{-1} polymer solutions in 1,2,3,4-tetrahydronaphthalene and spin-coated at 2000 rpm for 30 seconds.

Transistor Fabrication: Bottom-contact, top-gate (BC-TG) FETs and LEFETs were fabricated on glass substrates pre-cleaned in DECON 90 detergent solution, followed by sonication in

acetone and isopropanol. Source and drain electrodes were deposited by shadow-masked thermal evaporation in high vacuum (10^{-6} mbar). For the FETs, 40 nm thickness gold (Au) was used for both source and drain, with channel lengths varying between 30 and 100 μm and a constant width of 1000 μm. The Au electrodes were treated with an isopropanol solution of 2,3,4,5,6-pentafluorothiophenol (PFBT, purchased from Sigma-Aldrich) to form a self-assembled monolayer (SAM) prior to deposition of the organic semiconductor. For the LEFET devices, a PFBT SAM coated 40 nm thickness Au film was again used for the source, but 40 nm of Cs_2CO_3/Ag was used instead for the drain electrode. The organic semiconductor layer was deposited by spin coating at 2000 rpm for 30 seconds and was then annealed at 120 °C for 15 minutes. CYTOP (~ 900 nm thickness) was next spin-coated (as purchased, CYTOP CTL 809M from AGC Chemicals) as the dielectric layer. Finally, 20 nm of Al was evaporated through a shadow mask to form the top gate electrode. Thicknesses of the dielectric, semiconductor and electrode layers were measured using a Dektak Stylus Profilometer and transistor channel dimensions were checked using an optical microscope (Nikon Eclipse E600).

Electrical and Optical Characterization: The electrical and optical characteristics of the devices were measured in a dry nitrogen glovebox using an Agilent B2902A semiconductor parameter analyser and a probe-station fitted with two calibrated photodiodes positioned above and below the active region of the device (13,19). Electroluminescence and Photoluminance spectra were measured using an optical-fiber-coupled Ocean-Optics USB4000-XR spectrometer.

The device luminance was determined from the photodiode photocurrent, which in turn had been calibrated using an OLED pre-measured with a Konica Minolta LS-100 luminance meter. The emission zone area was calculated from the measured intensity profiles of microscopic images of the functioning devices, using the full width at half maximum values. The images were taken using a digital camera attached to the probe station. External quantum efficiency values were calculated using the photocurrent, source-drain current and emission spectrum, under the assumption that emission is Lambertian, as reported previously (13,19,24).

FET and LEFET charge carrier mobilities were determined from the electrical transfer characteristics in the saturation regime, using the following equation:

$$I_{DS} = \frac{W\,C_i}{2 \times L}(V_{GS} - V_{TH})^2$$

where I_{DS} is the experimentally measured source drain current, *W/L* is the channel width-to-length ratio, V_{GS} is the operating gate voltage and C_i is the geometrical capacitance of the bilayer dielectric. The resulting mobility values were adjusted for the non-ideality of the device characteristics using the reliability factor first proposed by Choi et al. (43), thereby yielding more readily comparable effective mobilities (see **Table S1**, **Supplementary Information**)

Structural Characterization: For X-ray diffraction (XRD) measurements, the organic semiconducting materials were spin-coated on heavily doped Si^{++} substrates. XRD patterns were obtained from a Rigaku Ultima diffractometer equipped with a Cu anode. Diffractograms were measured for C_8-BTBT, PDITTTT, and their blend. In order to quantify the XRD data, three prominent (002) diffraction peaks for each sample were fitted by Voigt curves (with both Lorentzian and Gaussian contributions). The Lorentzian broadening relates to the variations in vertical grain size (G_z), via the standard Scherrer formula, while the Gaussian broadening relates to microstrain (ε_s), which in turn relates to structural defects and the strain field around them (3); as such, the microstrain has been used as a measure of the lateral periodicity of the crystals (3). Note also that the instrumental broadening ($< 0.1^{\circ}$) was not taken-into-account in our analysis, so the reported G_z vales might be slightly overestimated.

Steady-state and time-resolved PL measurements were performed using a time-correlated single-photon counting apparatus (FluoTime 300, PicoQuant GmbH). Polymer and blend films on quartz substrates were excited at 10 MHz frequency using a 405 nm pulsed laser head, with detection wavelength set to 537 nm. The instrument response function (IRF) was taken into consideration in determining the decay times. After measuring the spectrum of excitation laser using a plain substrate, we conduct reconvolution of experimental data with IRF, and we process the biexponential fit to extract decay parameters for each sample.

Solid-state photoluminescence quantum efficiency (PLQE) measurements were performed with a Horiba Scientific FluoroMax-4 Spectrophotometer and Horiba Scientific Quantum-φ Integrating Sphere. Directly and Indirectly excited emission spectra were recorded for the samples and a blank substrate at a slit width of 0.9 nm. The PLQE was then calculated using the *de Mello* method (44), with the Jacobian correction applied to all wavelength/energy spectral conversions (45).

Supporting Information:

The Supporting Information is available free of charge on the website at DOI: xxxx or from

the authors.

References and Notes

1. A. J. Heeger, N. S. Sariciftci, E. B. Namdas, Semiconducting and Metallic Polymers. (*Oxford Univ. Press* 2011).

2. H. R. Tseng, H. Phan, C. Luo, M. Wang, L. A. Perez, S. N. Patel, L. Ying, E. J. Kramer, T. Q. Nguyen, G. C. Bazan, A. J. Heeger, High-mobility field-effect transistors fabricated with macroscopic aligned semiconducting polymers. *Adv. Mater.* **26**, 2993 (2014).

3. H. Kang, K. kook Han, J. E. Park, H. H. Lee, High mobility, low voltage polymer transistor. *Org. Electron.* **8**, 460 (2007).

4. J. Panidi, A. F. Paterson, D. Khim, Z. Fei, Y. Han, L. Tsetseris, G. Vourlias, P. A. Patsalas, M. Heeney, T. D. Anthopoulos, Remarkable Enhancement of the Hole Mobility in Several Organic Small-Molecules, Polymers, and Small-Molecule:Polymer Blend Transistors by Simple Admixing of the Lewis Acid p-Dopant $B(C_6F_5)_3$. *Adv. Sci.* **5**, 1, 1700290 (2018).

5. P.H. Wöbkenberg, J.G. Labram, J.-M. Swiecicki, K. Parkhomenko, D. Sredojevic, J.-P. Gisselbrecht, D. de Leeuw, D.D.C. Bradley, J.-P. Djukic, T.D. Anthopoulos, Ambipolar organic transistors and near-infrared phototransistors based on a solution-processable squarilium dye. *J. Mater. Chem.* **20**, 3673-3680 (2010).

6. S. Nam, H. Han, J. Seo, M. Song, H. Kim, T. D. Anthopoulos, I. McCulloch, D.D.C. Bradley, Y. Kim, Ambipolar Organic Phototransistors with p-Type/n-Type Conjugated Polymer Bulk Heterojunction Light-Sensing Layers. *Adv. Electronic Mater.* **2**, 1600264 (2016).

7. A. Hepp, H.Heil, W.Weise, M. Ahles, R. Schmechel, H. von Seggern, Light-Emitting Field-Effect Transistor Based on a Tetracene Thin Film. *Phys. Rev. Lett.* **91**, 157406 (2003).

8. W. S. C. Roelofs, W. H. Adriaans, R. A. J. Janssen, M. Kemerink, D. M. De Leeuw, Light Emission in the Unipolar Regime of Ambipolar Organic Field-Effect Transistors. *Adv. Funct. Mater.* **23**, 4133 (2013).

9. M. C. Gwinner, D. Kabra, M. Roberts, T. J. K. Brenner, B. H. Wallikewitz, C. R. McNeill, R. H. Friend, H. Sirringhaus, Highly efficient single-layer polymer ambipolar light-emitting field-effect transistors. *Adv. Mater.* **24**, 2728 (2012).

10. L. Burgi, M. Turbiez, R. Pfeiffer, F. Bienewald, H. J. Kirner, C. Winnewisser, High-mobility ambipolar near-infrared light-emitting polymer field-effect transistors. *Adv. Mater.* **20**, 2217 (2008).

11. J. Zaumseil, R. H. Friend, H. Sirringhaus, Spatial control of the recombination zone in an ambipolar light-emitting organic transistor. *Nat. Mater.* **5**, 69 (2006).

12. K. Tandy, M. Ullah, P. L. Burn, P. Meredith, E. B. Namdas, Unlocking the full potential of light emitting field-effect transistors by engineering charge injection layers. *Org. Electron.* **14**, 2953 (2013).

13. M. U. Chaudhry, K. Muhieddine, R. Wawrzinek, J. Li, S. C. Lo, E. B. Namdas, Nano-Alignment in Semiconducting Polymer Films: A Path to Achieve High Current Density and Brightness in Organic Light Emitting Transistors. *ACS Photonics* **5**, 2137 (2018).

14. F. Cicoira, C. Santato, Organic light emitting field effect transistors: advances and perspectives. *Adv. Funct. Mater.* **17**, 3421 (2007).

15. C. Zhang, P. Chen, W. Hu, Organic Light-Emitting Transistors: Materials, Device Configurations, and Operations. *Small,* **12**, 1252 (2016). M.

16. M. Muccini, W. Koopman, S. Toffanin, The photonic perspective of organic light-emitting tranistors. Laser Photonics Rev. **6**, 2, 258 (2012).

17. C. F. Liu, X. Liu, W. Y. Lai, W. Huang, Organic Light-Emitting Field-Effect Transistors: Device Geometries and Fabrication Techniques. Adv. Mater. **30**, 1802466 (2018).

18. R. Capelli, S. Toffanin, G. Generali, H. Usta, A. Facchetti, M. Muccini, Organic light-emitting transistors with an efficiency that outperforms the equivalent light-emitting diodes. *Nat. Mater.* **9**, 496 (2010).

19. M. Ullah, K. Tandy, S. D. Yambem, M. Aljada, P. L. Burn, P. Meredith, E. B. Namdas, Simultaneous enhancement of brightness, efficiency, and switching in RGB organic light emitting transistors. *Adv. Mater.* **25**, 6213 (2013).

20. T. Swager, Polymer light-emitting devices: Light from insulated organic wires. *Nat. Mater.* **1**, 151 (2002).

21. I. D. W. Samuel, G. A. Turnbull, Organic Semiconductor Lasers. *Chem. Rev.* **107**, 1272 (2007).

22. B. K. Yap, R. Xia, M. Campoy-Quiles, P. N. Stavrinou, D. D. C. Bradley, Simultaneous optimization of charge-carrier mobility and optical gain in semiconducting polymer films. *Nat. Mater.* **7**, 376 (2008).

23. J. Liu, H. Zhang, H. Dong, L. Meng, L. Jiang, L. Jiang, Y. Wang, J. Yu, Y. Sun, W. Hu, A. J. Heeger, High mobility emissive organic semiconductor. *Nat. Commun.* **6**, 10032 (2015).

24. M. Ullah, R. Wawrzinek, R. C. R. Nagiri, S. C. Lo, E. B. Namdas, UV–Deep Blue–Visible Light-Emitting Organic Field Effect Transistors with High Charge Carrier Mobilities. *Adv. Opt. Mater.* **5**, 8, 1600973 (2017).

25. T. Takenobu, S. Z. Bisri, T. Takahashi, M. Yahiro, C. Adachi, Y. Iwasa, High Current Density in Light-Emitting Transistors of Organic Single Crystals. *Phys. Rev. Lett.* **100**, 066601 (2008).

26. D. Venkateshvaran, M. Nikolka, A. Sadhanala, V. Lemaur, M. Zelazny, M. Kepa, M. Hurhangee, A. J. Kronemeijer, V. Pecunia, I. Nasrallah, I. Romanov, K. Broch, I. McCulloch, D. Emin, Y. Olivier, J. Cornil, D. Beljonne, H. Sirringhaus, Approaching disorder-free transport in high-mobility conjugated polymers. *Nature* **515**, 384 (2014).

27. K. Zhao, O. Wodo, D. Ren, H. U. Khan, M. R. Niazi, H. Hu, M. Abdelsamie, R. Li, E. Q. Li, L. Yu, B. Yan, M. M. Payne, J. Smith, J. E. Anthony, T. D. Anthopoulos, S. T. Thoroddsen, B. Ganapathysubramanian, A. Amassian, *Adv. Funct. Mater*. 26, 1737 (2016).

28. Alexandra F. Paterson Neil D. Treat Weimin Zhang Zhuping Fei Gwenhivir Wyatt-Moon Hendrik Faber George Vourlias Panos A. Patsalas Olga Solomeshch Nir Tessler Martin Heeney Thomas D. Anthopoulos. *Adv. Mater*. 28, 35. 7791 (2016).

29. Alexandra F. Paterson Leonidas Tsetseris Ruipeng Li Aniruddha Basu Hendrik Faber Abdul-Hamid Emwas Julianna Panidi Zhuping Fei Muhammad R. Niazi Dalaver H. Anjum Martin Heeney Thomas D. Anthopoulos. *Adv. Mater*. 31, 27, 1900871 (2019).

30. J. Kang, N. Shin, Y. J. Do, V. M. Prabhu, D. Y. Yoon, Structure and properties of small molecule− polymer blend semiconductors for organic thin film transistors. *J. Am. Chem. Soc.* **130**, 12273 (2008).

31. J. Smith, R. Hamilton, I. McCulloch, N. Stingelin-Stutzmann, M. Heeney, D. D. C. Bradley, T. D. Anthopoulos, Solution-processed organic transistors based on semiconducting blends. *J. Mater. Chem.* **20**, 2562 (2010).

32. T. Uemura, Y. Hirose, M. Uno, K. Takimiya, J. Takeya, Very high mobility in solution-processed organic thin-film transistors of highly ordered [1] benzothieno [3, 2-b] benzothiophene derivatives. *App. Phys. Exp.* **02**, 11, 111501 (2009).

33. T. Virgili, D. G. Lidzey, D. D. C. Bradley, Efficient Energy Transfer from Blue to Red in Tetraphenylporphyrin-Doped Poly (9, 9-dioctylfluorene) Light-Emitting Diodes. *Adv. Mater.* **12**, 58 (2000).

34. Q. Zhang, J. Liu, Q. Wei, X. Guo, Y. Xu, R. Xia, L. Xie, Y. Qian, C. Sun, L. Lüer, J. Cabanillas-Gonzalez, D. D. C. Bradley, W. Huang, Host Exciton Confinement for Enhanced Förster-Transfer-Blend Gain Media Yielding Highly Efficient Yellow-Green Lasers. *Adv. Funct. Mater.* **28**, 17, 1705824 (2018).

35. W. Mitchell, M. D'lavari, C. Wang, D. Sparrowe. *World Intellectual Property Organization*, patent application WO 2015/058827 (2015).

36. Y. J. Cheng, S. W. Cheng, C. Y. Chang, W. S. Kao, M. H. Liao, Chain-Shu Hsu, Diindenothieno[2,3-b]thiophene arene for efficient organic photovoltaics with an extra high open-circuit voltage of 1.14 ev. *Chem. Comm.* **48**, 26 (2012).

37. M. C. Gather, S. Reineke, Recent advances in light outcoupling from white organic light-emitting diodes. *J. Photonics Energy* **5**, 057607 (2015).

38. A. Salehi, Y. Chen, X. Fu, C. Peng, F. So, Manipulating Refractive Index in Organic Light-Emitting Diodes. *ACS Appl. Mater. Interfaces* **10**, 9595 (2018).

39. T. Matsushima, A. S. D. Sandanayaka, Y. Esaki, C. Adachi, Vacuum-and-solvent-free fabrication of organic semiconductor layers for field-effect transistors. *Sci. Rep.* **5**, 14547 (2015).

40. Z. Zhang, B. Peng, X. Ji, K. Pei, P. K. L. Chan, Marangoni-Effect-Assisted Bar-Coating Method for High-Quality Organic Crystals with Compressive and Tensile Strains. *Adv. Funct. Mater.* **27**, 37, 1703443 (2017).

41. J. Smith, R. Hamilton, Y Qi, A. Kahn, D. D. C. Bradley, M. Heeney, I. McCulloch, T. D. Anthopoulos, The Influence of Film Morphology in High-Mobility Small-Molecule: Polymer Blend Organic Transistors. *Adv. Funct. Mater.* **20**,14, 2330 (2010).

42. H. H. Choi, K. Cho, C. D. Frisbie, H. Sirringhaus, V. Podzorov, Critical assessment of charge mobility extraction in FETs. *Nat. Mater.* **17**, 2 (2017).

43. T. Uemura, C. Rolin, T. H. Ke, P. Fesenko, J. Genoe, P. Heremans, J. Takeya, On the Extraction of Charge Carrier Mobility in High-Mobility Organic Transistors. *Adv. Mater.* **28**, 151 (2016).

44. J. C. de Mello, H. F. Wittmann, R. H. Friend, An improved experimental determination of external photoluminescence quantum efficiency. *Adv. Mater.* **9**, 230 (1997).

45. J. Mooney, P. Kambhampati, Correction to "Get the Basics Right: Jacobian Conversion of Wavelength and Energy Scales for Quantitative Analysis of Emission Spectra". *J. Phys. Chem. Lett.* **5**, 3497 (2014).

Figures and Tables
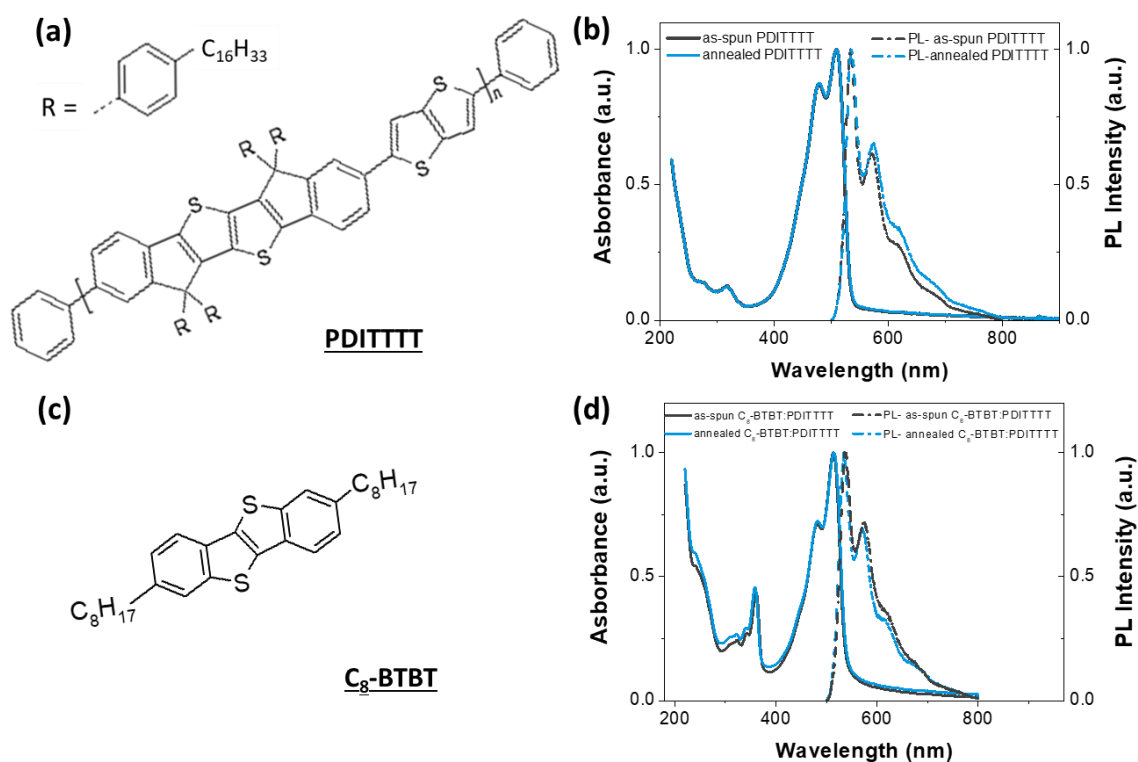
Fig. 1: Chemical structure of (a) PDITTTT polymer and (c) C_8-BTBT small molecule. Normalised photoluminescence (PL) and absorption spectra for (b) PDITTTT polymer and (d) C_8-BTBT: PDITTTT blend films. The solid lines (left ordinate) are absorption and the dashed lines (right ordinate) are the PL, for as spin-coated (black) and for post annealing (blue) thin films.
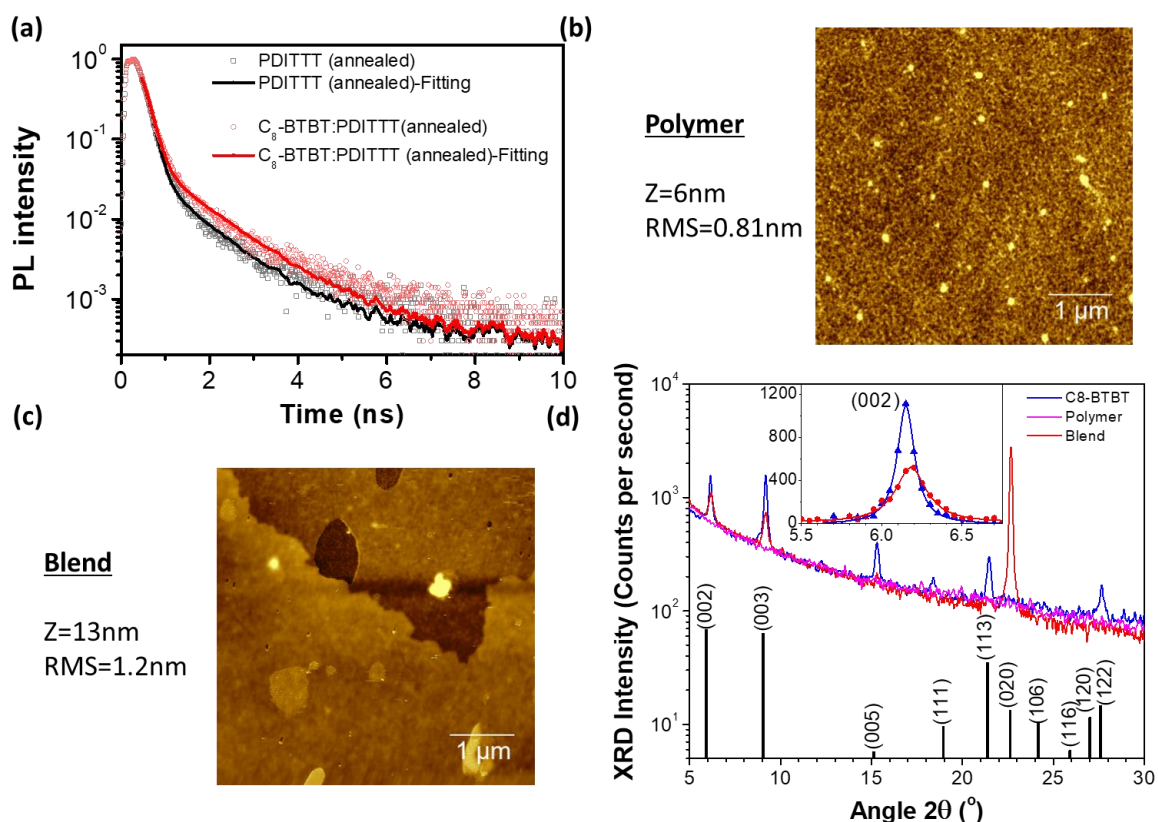
Fig. 2: (a) Normalized time-resolved PL (537 nm, pumped at 405nm) for annealed PDITTTT polymer and C_8-BTBT: PDITTTT blend films. Topographic AFM images of the (b) polymer only and (c) C_8-BTBT: PDITTTT blend. Z is the height scale. Root mean square roughness values were determined for each image, with 0.81 nm for the polymer and 1.3 nm for the blend. (d) XRD patterns for PDITTTT polymer (magenta line), C_8-BTBT (blue line), and their blend (red line). The inset shows details of the (002) basal peak for C_8-BTBT (blue symbols) and its blend with PDITTTT (red symbols) together with Voigt fits (lines of the same colour). Also shown at the bottom of the panel is a powder diffractogram for C_8-BTBT with indexing of the peaks based on powder diffraction data (34).
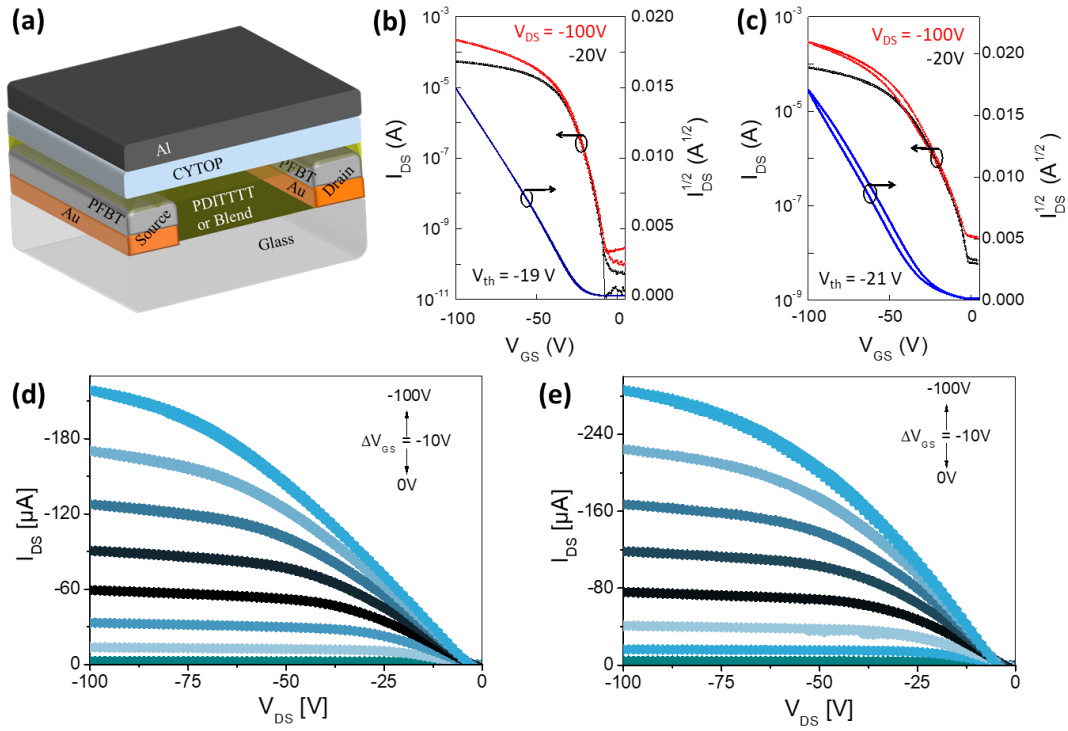
Fig. 3: (a) BC-TG FET architecture using Au/PFBT electrodes. The FET transfer characteristics for the PDITTTT and C_8-BTBT: PDITTTT blend are given in (b) and (C), where the red line show transfer curves in saturation mode (V_{DS}= -100V) and black lines in linear regime (V_{DS}= -20V). The output curves for the PDITTTT and C_8-BTBT: PDITTTT blend are given in (d) and (e) respectively. The devices had a channel length (L) and width (W) of 50 and 1000 μm, respectively.
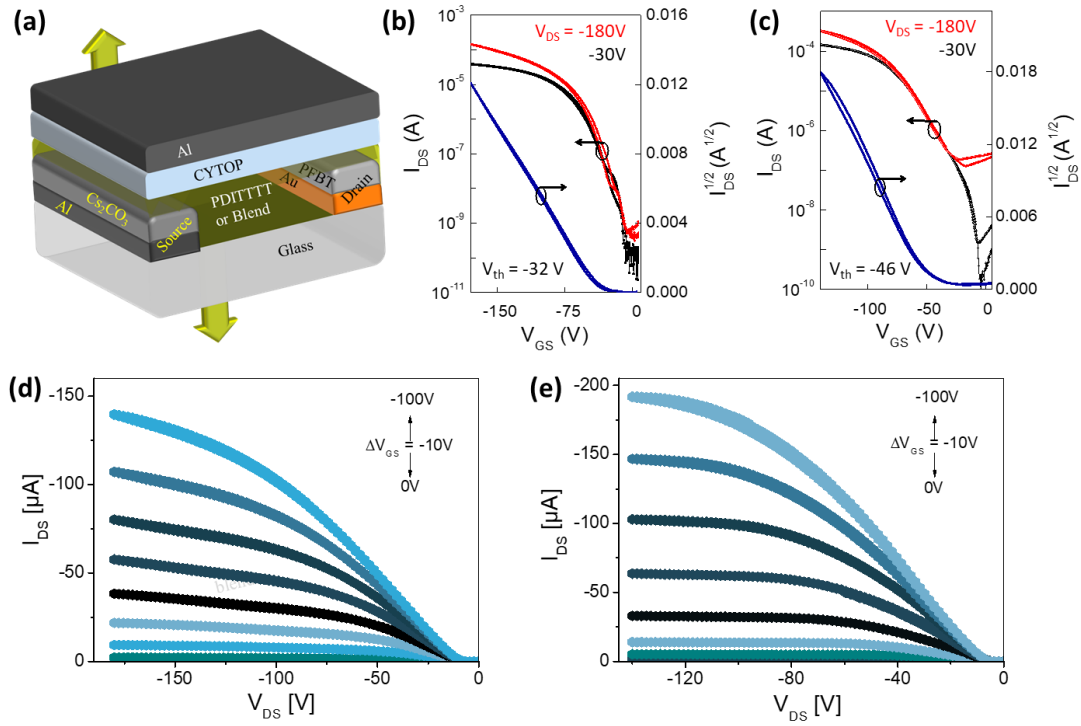
Fig. 4: (a) BC-TG LEFET architecture. Also shown are the LEFET transfer characteristics (b) for the PDITTTT polymer and (c) C_8-BTBT: PDITTTT blend. The red line show transfer curves in saturation mode (V_{DS}= -180V) and black lines in linear regime (V_{DS}= -30V). The output curves for the PDITTTT and C_8-BTBT: PDITTTT blend are given in (d) and (e) respectively. The devices had a channel length (L) and width (W) of 140 μm 652 μm, respectively.
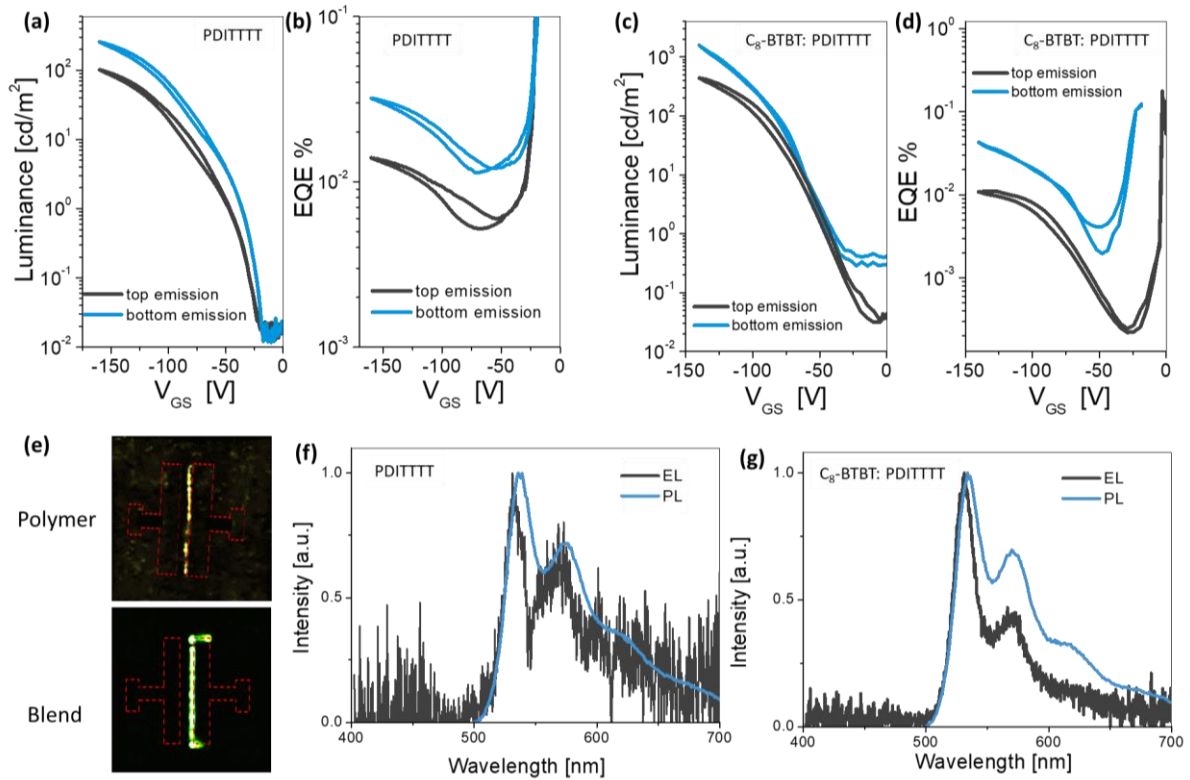
Fig. 5: (a), (b), (c) and (d) Luminance and EQE voltage dependence for PDITTTT polymer ((a) and (b)) and C_8-BTBT: PDITTTT blend ((c) and (d)) LEFETs. Data are presented for both top (black lines) and bottom (blue lines) emission. Also shown are (e) microscope emission images and (f) and (g) electroluminescence spectra (black line) for polymer ((f)) and blend ((g)) devices. In (e) the red dashed lines show an outline of the source and drain electrodes. PL spectra (blue lines) are shown in (f) and (g) for comparison with the EL data.

18

Table 1: <u>Summary of results and comparison with reported polymer LEFETs:</u> The plus/minus values represent the standard deviation on the mean as derived from the average of 6 devices.

	This study				Ref #8	Ref #9	Ref #10	Ref #12
	Polymer		Blend		Polymer	Polymer	Polymer	Polymer
Device Architecture	3-terminal 1-layer Bottom Emission	3-terminal 1-layer Top Emission	3-terminal 1-layer Bottom emission	3-terminal 1-layer Top emission	3-terminal 1-layer Top emission	3-terminal 1-layer Top emission	3 terminal 1-layer Top emission	3-terminal 1-layer Top emission
Polymer Material	PDITTTT		C$_8$-BTBT: PDITTTT :		PDPPTPT	F8BT	BBTDPP1	PDY-132 Super Yellow
$\mu_{hole\,-Sat}$ **(cm^{2}V^{-1}s^{-1})**	0.6 ± 0.1 ($\mu_{hole\,-eff}$ =0.42)		7 ± 1 ($\mu_{hole\,-eff}$ =3.2)		~ 0.02	Not given $<10^{-3}$	0.1	1×10^{-4}
$\mu_{electron}$ **(cm^{2}V^{-1}s^{-1})**	-	-	-	-	~ 0.02	- ($<10^{-3}$)	0.09	4×10^{-4}
ON/OFF Ratio	$> 10^5$	$> 10^5$	$> 10^3$	$> 10^3$	$> 10^5$	< 10	$> 10^3$	$<10^4$
Luminance (cd/m^2)	$\sim 300 \pm 100$	$\sim 100 \pm 25$	$\sim 1600 \pm 300$	$\sim 550 \pm 100$	-	~ 4000	-	~150
EQE (%)	0.035 ± 0.01	0.01 ± 0.002	0.045 ± 0.01	0.01 ± 0.02	~ 0.07	4	$\sim 10^{-5}$	0.14

Supporting Information for

Polymer light-emitting transistors with charge carrier mobilities exceeding 1 cm² V⁻¹ s⁻¹

Mujeeb Ullah Chaudhry[*1], *Julianna Panidi*[2], *Sungho Nam*[3], *Alice Smith*[3], *Jongchul Lim*[3], *Kornelius Tezner*[2], *Panos A. Patsalas*[4], *George Vourlias*[4], *Wai-Yu Sit*[2], *Yuliar Firdaus*[5], *Martin H. Heeney*[6], *Donal D. C. Bradley*[*3,7], *Thomas D. Anthopoulos*[*2,5]

[1] Department of Engineering, Durham University, Durham, DH1 3LE, United Kingdom
[2] Blackett Laboratory, Department of Physics & Centre for Plastic Electronics, Imperial College London, London SW7 2BW, United Kingdom
[3] Department of Physics, University of Oxford, Oxford OX1 3PU, United Kingdom
[4] Prof. P. A. Patsalas, Prof. G. Vourlias, Department of Physics, Laboratory of Applied Physics Aristotle University of Thessaloniki, GR-54124, Greece
[5] Physical Science and Engineering Division, King Abdullah University of Science and Technology, Thuwal 23955, Saudi Arabia
[6] Department of Chemistry & Centre for Plastic Electronics, Imperial College London, London SW7 2BW, United Kingdom
[7] Department of Engineering Science, University of Oxford, Oxford OX1 3PJ, United Kingdom,

* Correspondence: mujeeb.u.chaudhry@durham.ac.uk (MUC), donal.bradley@mpls.ox.ac.uk (DDCB), thomas.anthopoulos@kaust.edu.sa (TDA)

Fig. S1. PL and absorbance spectra of the C_8-BTBT film.

Measurement of PLQE

Fig. S2. PLQE and Absorption against sample composition.

Table-S1. Numerical values of PLQE & Absorption and integration ranges used to determine P (emission) and L (excitation) areas.

Fig. S3. Integration ranges used to determine P (emission) and L (excitation) areas.

Fig. S4. Refractive index vs. wavelength of as-spun and annealed polymer film.

Fig.S5. Refractive index vs. wavelength of as-spun and annealed small molecule (C_8-BTBT) film.

Fig. S6. Refractive index vs. wavelength of as-spun and annealed C_8-BTBT:PDITTTT film.

Fig. S7. Times resolved PL of annealed PDITTTT film.

Fig. S8. Times resolved PL of annealed C_8-BTBT:PDITTTT film.

Figure S9. Height histograms of the AFM images provided in **Figure 2.**

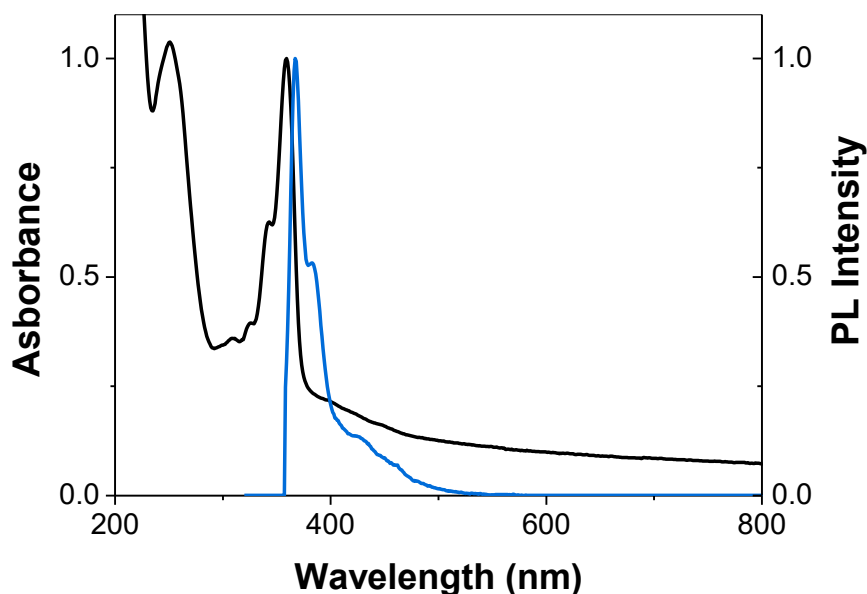**Calculation of Reliability factor and effective mobility**

Figure S1. Absorbance (normalized to absorption peak at 359 nm) and PL spectra of C_8-BTBT film.

Measurements of Photoluminescence Quantum Efficiency (PLQE):

The de Mello method [39] involves recording three spectra to calculate PLQE:

1. Blank: No sample placed in sphere and excitation beam placed in indirect position.
     Indirect Excitation: Sample placed in sphere away from the first pass of the excitation beam. Any emission is due to absorption of the reflected excitation beam.

Direct Excitation: Sample placed in sphere directly in the path of the excitation beam. Emission due to absorption from this direct excitation as well as any absorption from reflections.

Figure S8. Integrating sphere experiments required to calculate PLQE using the de Mello method.

The absorption, A, and PLQE were calculated using equations (1) & (2), where L is the area under the excitation peak and P is the area under the emission peak for the denoted experiment. To determine these L and P values, the spectra were baselined and converted to Energy with the Jacobian correction applied (2).

$$A = 1 - \frac{L_3}{L_2} \qquad (1)$$

$$PLQY = \frac{P_3 - (1-A)P_2}{L_1 A} \qquad (2)$$

A = absorption of sample, P2 = area under indirect emission peak, P3 = area under direct emission peak, L1 = area under blank excitation peak, L2 = area under indirect excitation peak, L3 = area under direct excitation peak
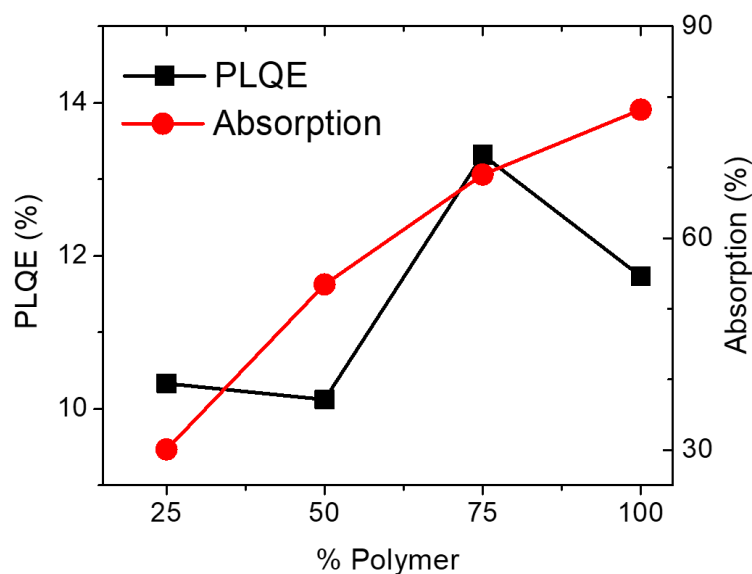
Figure S2. PLQE and absorption against sample composition (percentage fraction of polymer, PDITTTT).

Table-S1. Numerical values of PLQE & Absorption and integration ranges used to determine P (emission) and L (excitation) areas.

C$_8$BTBT:PDITTTT	% PDITTTT	A	PLQE	Integration Ranges (eV)			
				Excitation Low	Excitation High	Emission Low	Emission High
3:1	25	0.30	10.3%	2.427	2.567	2.081	2.422

22

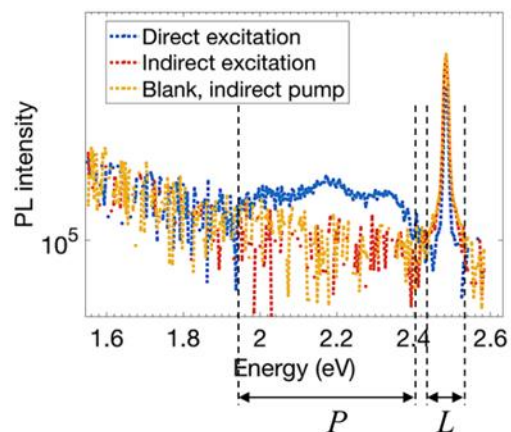| 1:1	50	0.53	10.1%	2.441	2.541	2.046	2.436
1:3	75	0.69	13.3%	2.441	2.541	2.046	2.436
0:1	100	0.78	11.7%	2.441	2.541	1.968	2.436
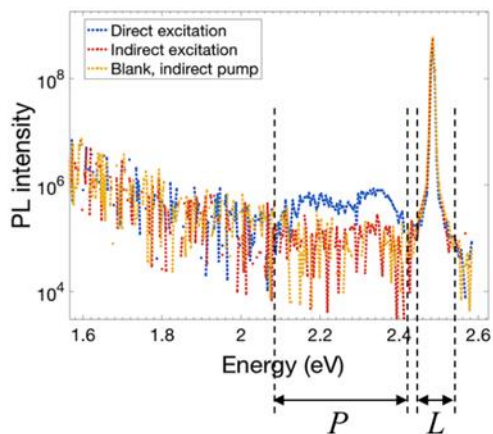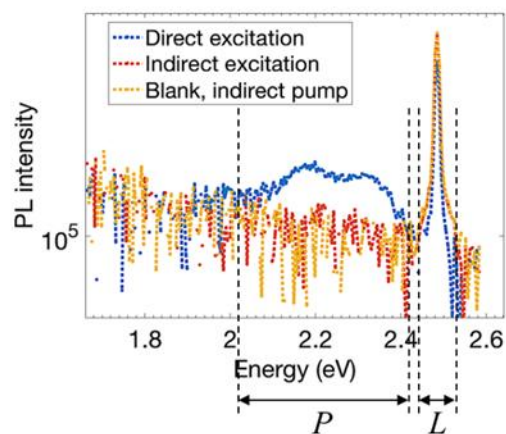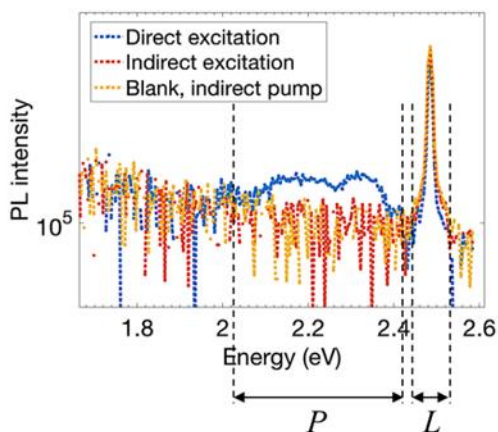
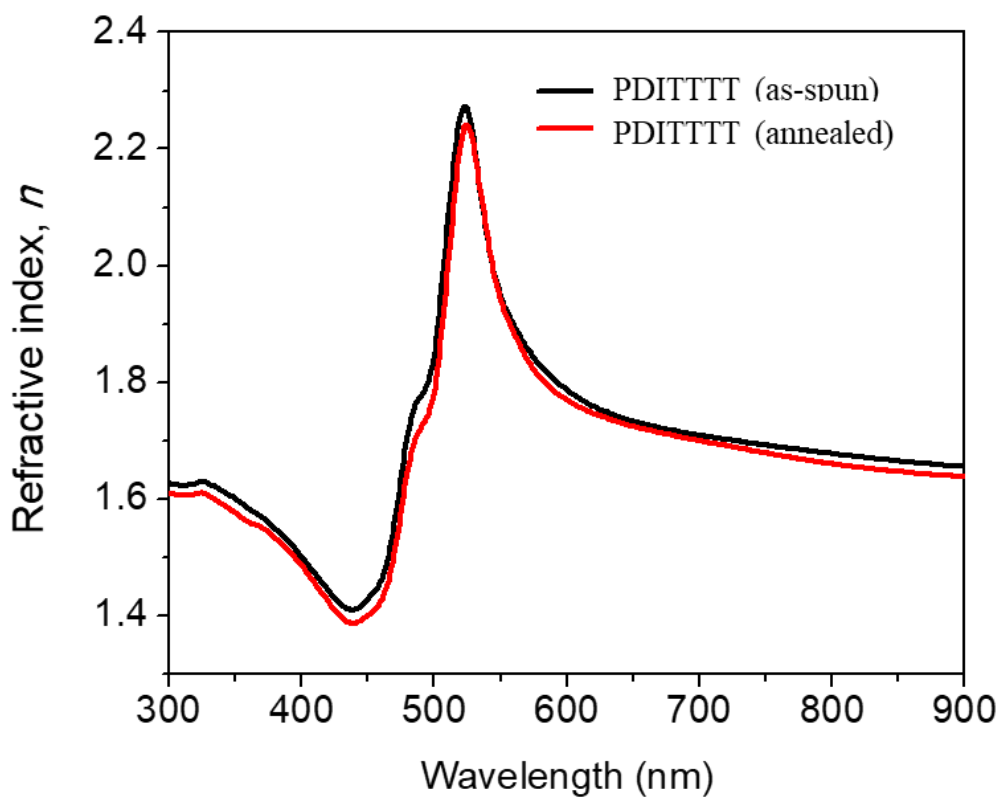**Figure S3.** Integration ranges used to determine P (emission) and L (excitation) areas.

Figure S4. Refractive index vs. wavelength of as-spun and annealed polymer film.
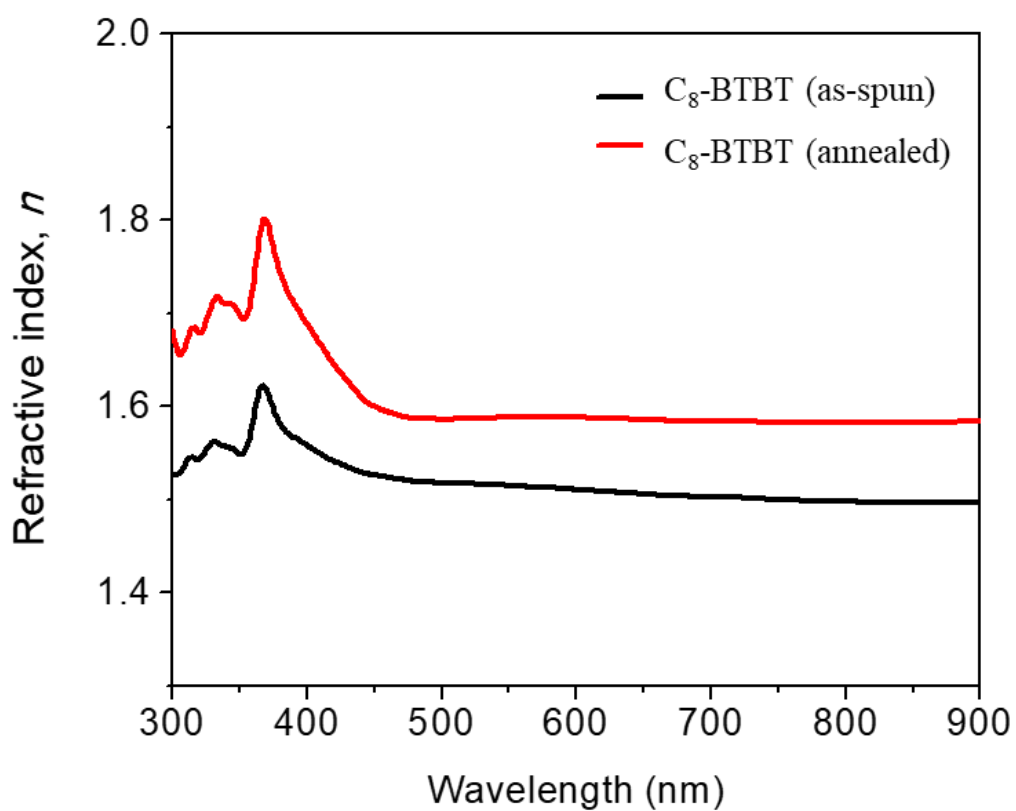

Figure S5. Refractive index vs. wavelength of as-spun and annealed small molecule (C_8-BTBT) film.
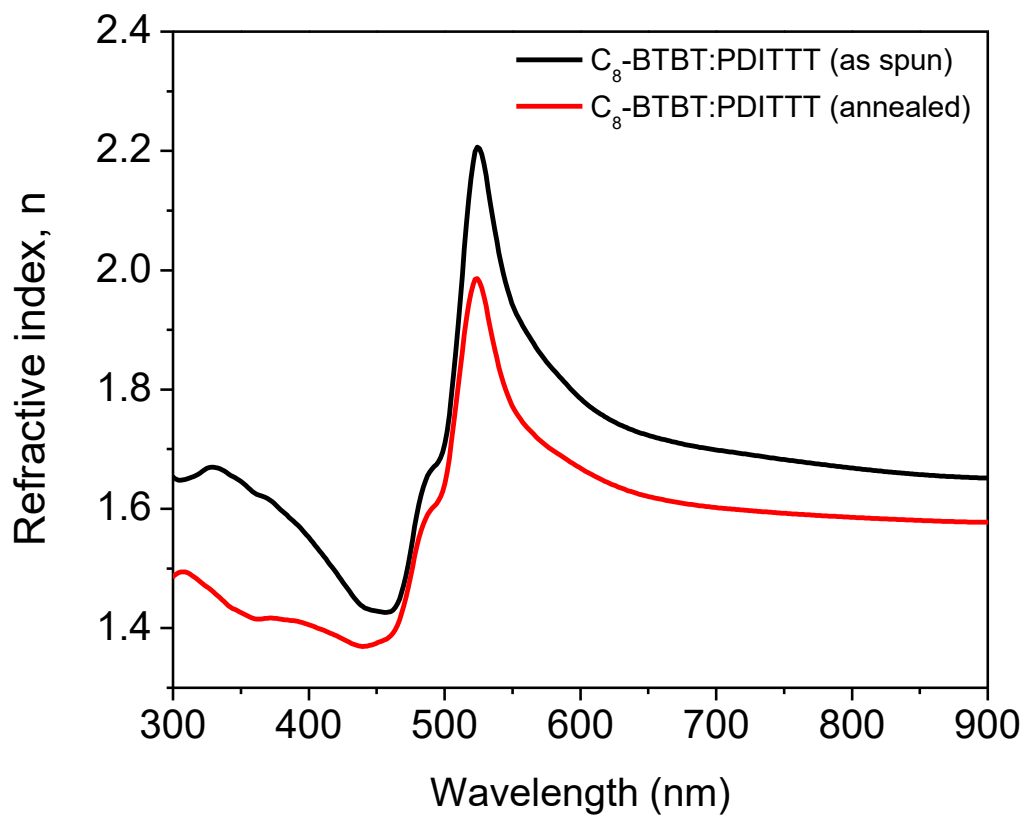
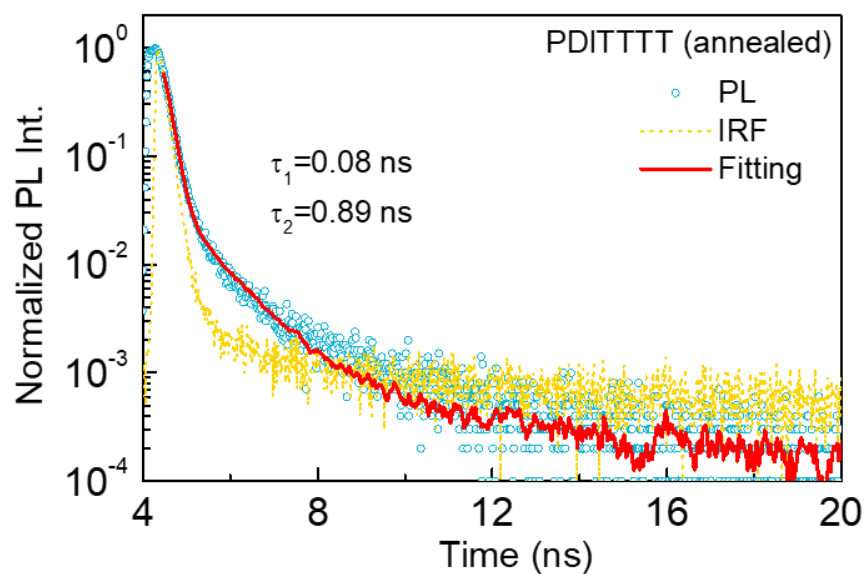**Figure S6.** Refractive index vs. wavelength of as-spun and annealed C_8-BTBT:PDITTTT film.

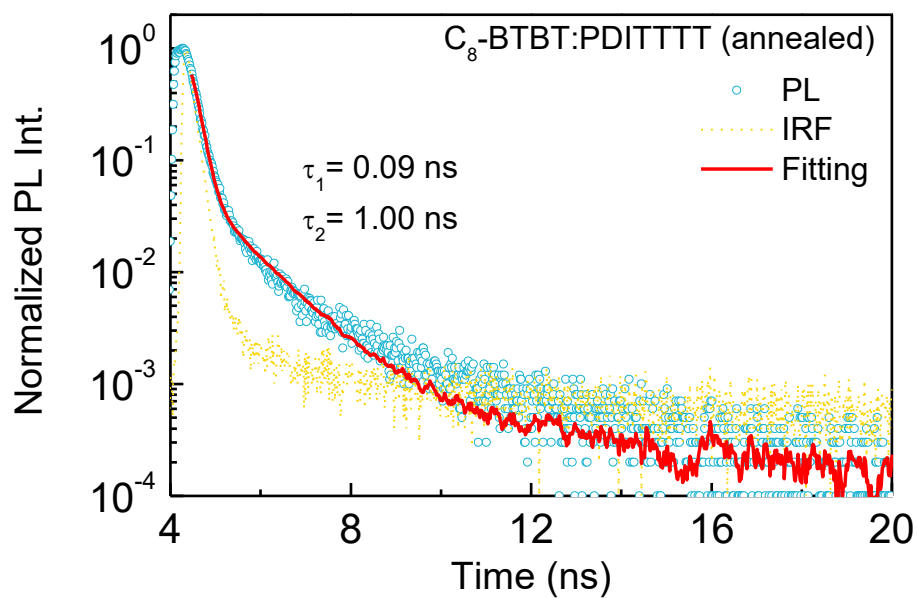**Figure S7.** Times resolved PL of annealed PDITTTT film.

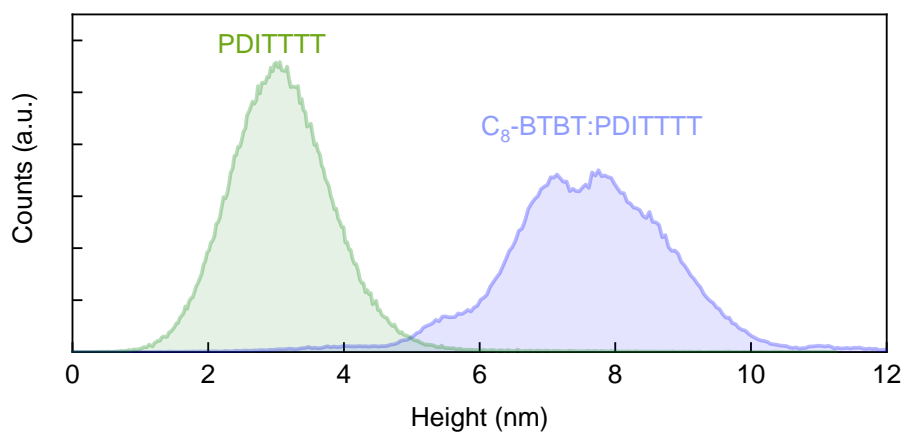**Figure S8.** Times resolved PL of annealed C_8-BTBT:PDITTTT film.

Figure S9. Height histograms of the AFM images provided in **Figure 2.**

Calculation of reliability factor and effective mobility:

The measurement reliability factor* 'r' is determines the behaviour of reported FETs follows the physics of the simple linear increase of conductivity with carrier density under the assumption of a constant mobility and negligible threshold voltage. It is defined as the ratio of the maximum channel conductivity experimentally achieved in a FET at the maximum gate voltage to the maximum channel conductivity expected in a correctly functioning ideal FET with the calculated carrier mobility μ and identical other device parameters at the same maximum gate voltage. Reliability factor, "r" can be calculated from the calculated "μ", the stated device parameters and the FET characteristics. In the saturation regime, equation (3) shows that the reliability factor is:

$$r_{sat} = \left[\frac{\sqrt{|I_{SD}|^{max}} - \sqrt{|I_{SD}|^0}}{|V_{GS}|^{max}} \right]^2 \Bigg/ \left[\frac{WC_i}{2L} \mu_{sat} \right]_{calculated}$$

$$= \left[\frac{\sqrt{|I_{SD}|^{max}} - \sqrt{|I_{SD}|^0}}{|V_{GS}|^{max}} \right]^2 \Bigg/ \left[\frac{\partial \sqrt{|I_{SD}|}}{V_{GS}} \right]^2_{calculated} \qquad (3)$$

Here, μ_{sat} is the calculated mobility, L, W and C_i are the device parameters, and $|I_{SD}|^{max}$ is the experimental maximum source–drain current reached at the maximum gate voltage $|V_{GS}|^{max}$. And $|I_{SD}|^0$ denotes the source–drain current at $V_{GS} = 0$.

The effective mobility is calculated from the reliability factor, where reliability factor is 100%. The effective mobility can be also calculated from reliability factor and claim mobility from the equation (4),

$$\mu_{eff} = r \times \mu_{calculated} \qquad (4)$$

Table-S2. Calculated mobility, reliability factor and effective mobility calculation.

Devices		μ_{sat} (cm^2 V^{-1} s^{-1})		μ_{eff} (cm^2 V^{-1} s^{-1})
		$\mu_{calculated}$	r %	
PDITTTT	OFET	1	63 %	0.63
	LEFET	0.6	70 %	0.42
C$_8$BTBT:PDITTTT	OFET	1.6	51 %	0.82
	LEFET	7	56 %	3.2

Measurement of electron mobility:

Electron mobilities were measured space charge limiting current (SCLC) formulation using a diode configuration of glass/Al/Cs$_2$CO$_3$/(polymer or blend)/Cs$_2$CO$_3$/Al. By taking the dark current density in the range of 0-8 V and fitting the results to a space charge limited equation (5).

$$J = \frac{9 \, \epsilon_o \, \epsilon_r \, \mu_o \, V^2}{8 \, L^3} \; exp\left(0.89\beta \; \sqrt{\frac{V}{L}} \right) \qquad (5)$$

where J is the current density, L is the film thickness of the active layer, μ_o is the hole mobility, ε_r is the relative dielectric constant of the transport medium, ε_o is the permittivity of free space (8.85×10^{-12} F/m), V (= V$_{appl}$ − V$_{bi}$) is the internal voltage in the device, where V$_{appl}$ is the applied voltage to the device and V$_{bi}$ is the built-in voltage due to the relative work function difference of the two electrodes.
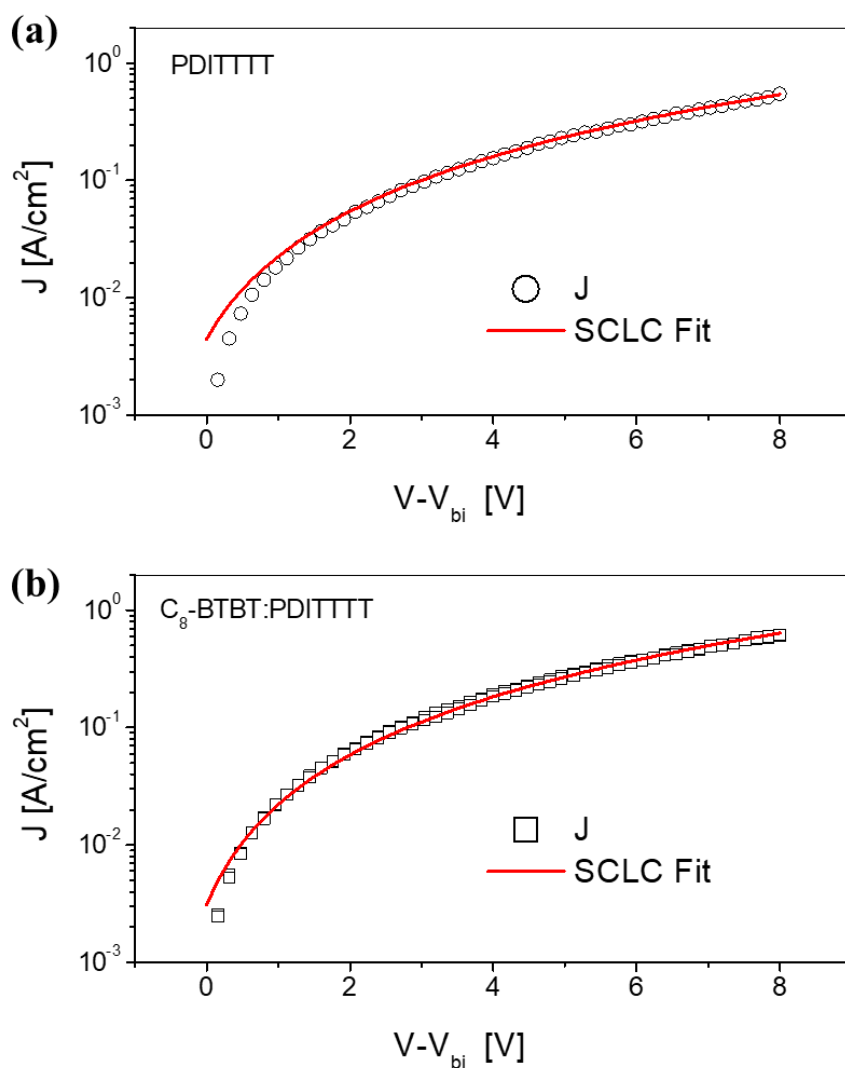
Figure S10. Dark-current densities and SCLC fitting in electron-only diode structure using: (a) neat films; b) blend films. The solid red lines represent the best fits to SCLC model and the open circles/squares are the experimental data. Extracted mobilities from the fitting were 5.6 $\times 10^{-8}$ cm^2 V^{-1} s^{-1} in polymer PDITTTT films 6 $\times 10^{-8}$ cm^2 V^{-1} s^{-1} in blend C$_8$-BTBT:PDITTTT films.
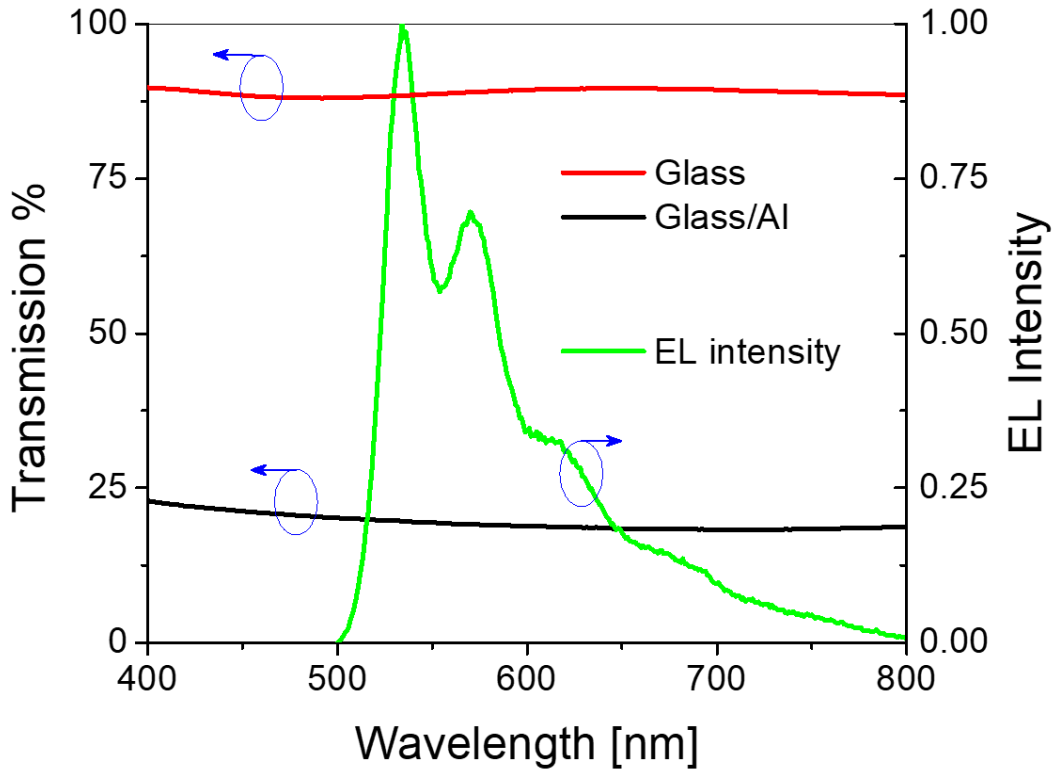
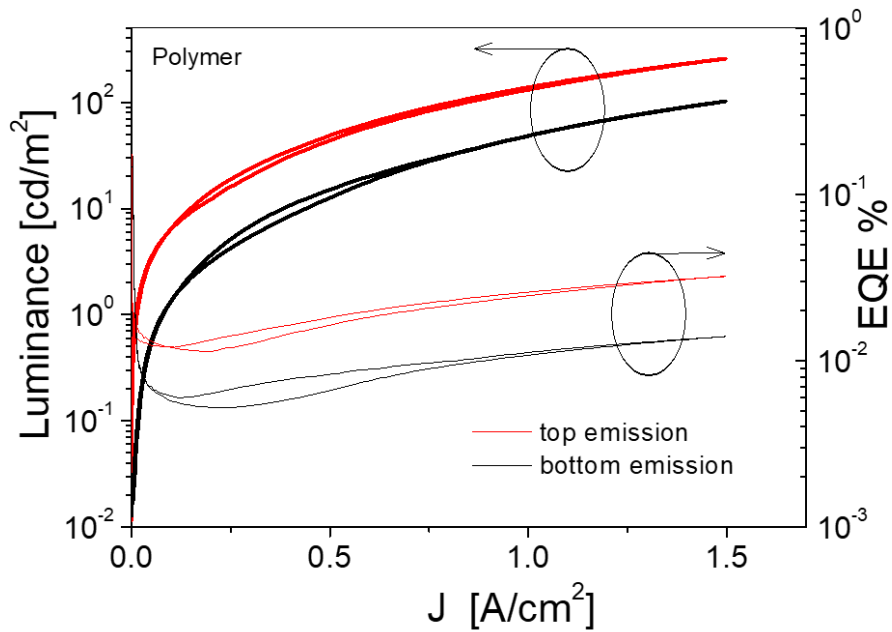**Figure S11.** Transmittance of bottom glass and top Al gate electrode.

Figure S12. Luminance and EQE as function of current density of polymer LEFETs.
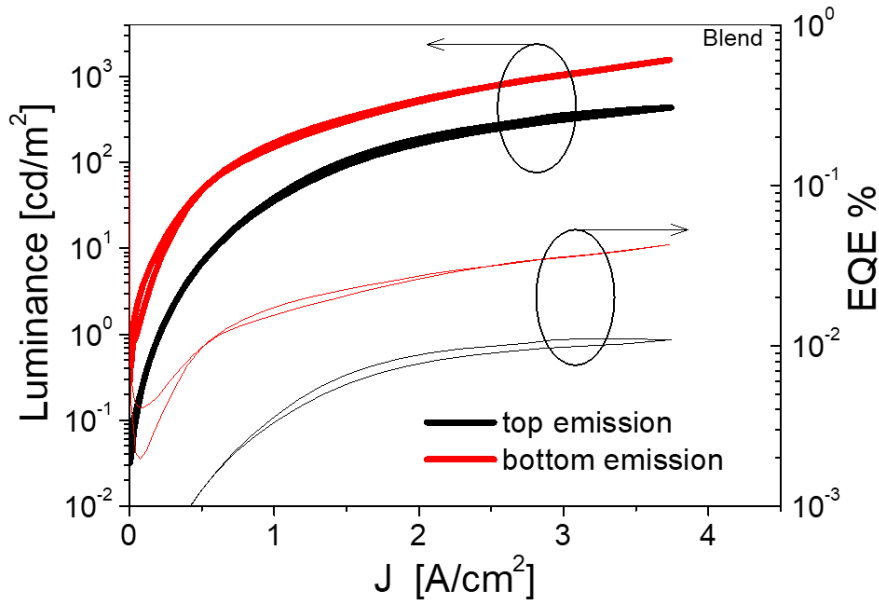

Figure S13. Luminance and EQE as function of current density of blend LEFETs.
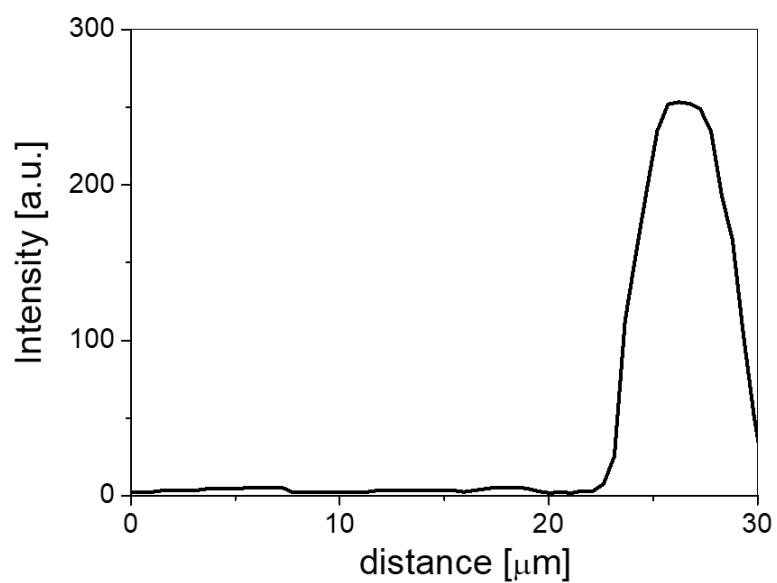
Figure S14. Image intensity profile and FWHM of polymer PDITTTT based LEFETs.

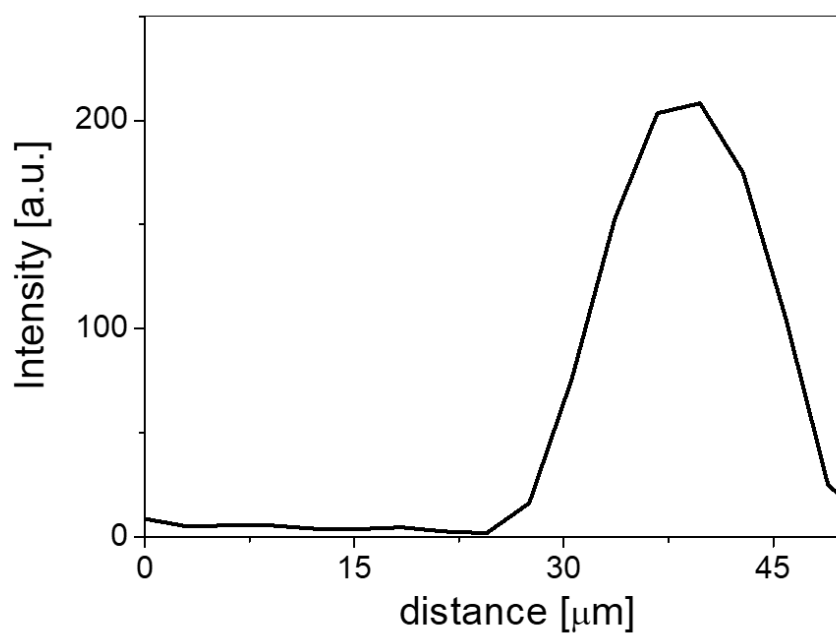**Figure S15.** Image intensity profile and FWHM of C_8-BTBT:PDITTTT based LEFETs.
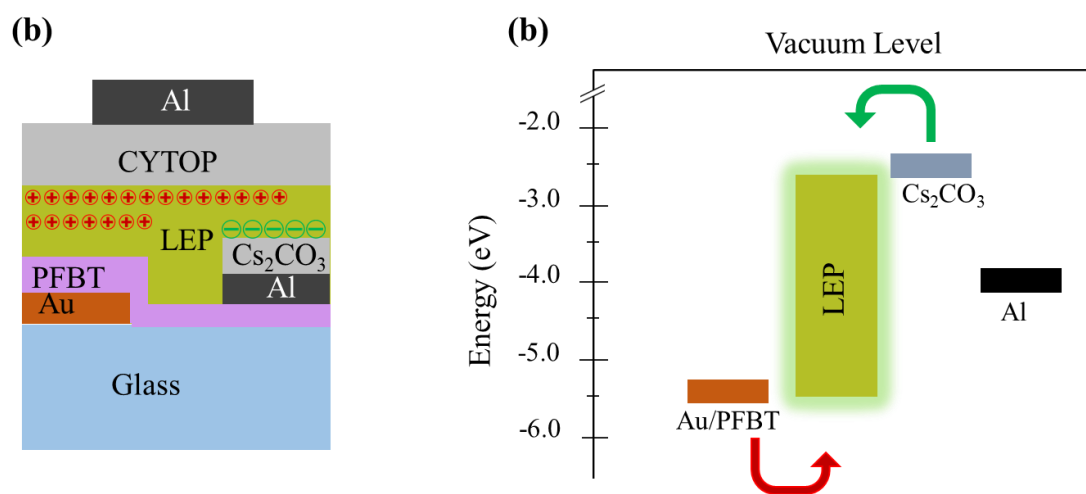
(b)

(b)

Figure S16. (a) Working mechanism of the LEFET, where LEP is light emitting polymer films (pristine or blend) and (**b**) energy level diagram.

Calculating recombination efficiency (internal quantum efficiency):

Electrons and the holes are injected from source and drain electrodes and move across the FET channel under the influence of the lateral source-drain electric field. These moving charges are probable to form singlet state excitons and triplet state excitons and eventually recombine to emit light. The efficiency of light emission is given by equation 6:

$$\varphi_{EQE} = \varphi_{escape} \times \varphi_{capture} \times \varphi_{spin} \times \varphi_{PLQE} \qquad (6)$$

where $\varphi_{capture}$ (recombination efficiency) is the fraction of electrons and holes that recombine to form excitons, φ_{EQE} is the calculated EQE, φ_{escape} is the fraction of photons that can escape from the device, φ_{spin} is the factor allowed due to spin statistics and Φ_{PLQE} is the photoluminescence quantum yield (PLQE) in the solid state. The percentage of photons that can escape from device, φ_{escape}, is approximately $1/2n^2$ (where n is the refractive index of the polymer film is 2.2 and blend films is 1.95 at peak emission wavelength). Polymer is a singlet emitter and so $\varphi_{spin} = 0.25$. Calculated recombination efficiency for all the devices is given below in **Table-S3**.

Table-S3. Recombination Efficiencies.

Parameters	Polymer	Blend
PLQE	11.7 %	13.3 %
EQE at maximum brightness [%]	0. 035 %	0.045 %
Recombination Efficiency at maximum brightness [%]	5.8 %	5.1 %

Table-S4. A comparison of the results of single-layer LEFETs previously reported and this study.

|	This study		Ref #1	Ref #1	Ref #2	Ref #3	Ref #4	Ref #5	Ref #6	Ref #7
Device Architecture	3 terminal 1-layer	3 terminal 1-layer	3 terminal 1-layer	3 terminal 1-layer	3 terminal 1-layer	3-terminal 1-layer	3-terminal 1-layer	3-terminal 1-layer	3-terminal 1-layer	3 terminal 1-layer
Material	Polymer	Polymer Blend	BTBT-C_{10}	Ph-BTBT-C_{10}	F8BT	rubrene & tetracene (single crystals)	EFIN	BSB-Me (single crystal)	P3V2 (single crystal)	SY
μ_{hole} (cm^{2}V^{-1}s^{-1})	1	1	6	2	- ($<10^{-3}$)	0.82 & 2.3	6×10^{-6}	1×10^{-4}	1.1×10^{-1}	1×10^{-4}
$\mu_{electron}$ (cm^{2}V^{-1}s^{-1})	-	-	-	-	- ($<10^{-3}$)	0.27 & 0.12	-	1×10^{-2}	1.3×10^{-2}	4×10^{-4}
ON/OFF Ratio	~10^6	~10^6	~10^9	~10^7	<10	~10^2 & ~10^5	~10^4	<10^4	<10^4	<10^4
EQE at maximum emission intensity (%)	0.046	0.04	0.003	0.0006	4	0.002 & 0.02	Not reported	Not reported	Not reported	0.14

35
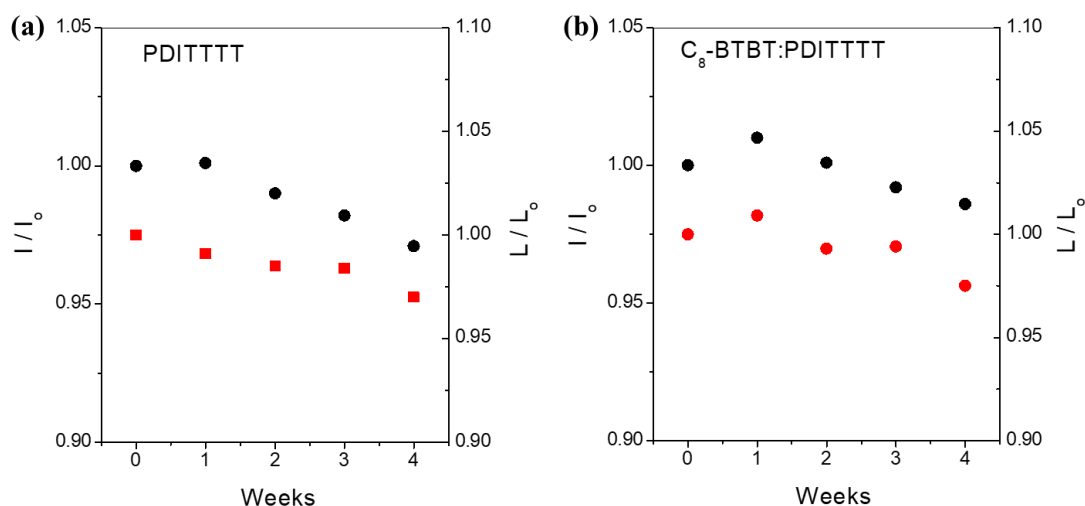
Figure S17. Normalized Source drain current (black circles) and luminance ratio (red circles) of (**a**) PDITTTT and (**b**) C_8-BTBT:PDITTTT films based LEFET. Samples were stored in ambient for a week and tested.

References:

1. 22 Mujeeb Ullah, Robert Wawrzinek, Ravi Chandra Raju Nagiri, Shih-Chun Lo, and Ebinazar B. Namdas. **UV-deep blue-visible light emitting organic field effect transistors with high charge carrier mobilities.** Adv. Opt. Mater. **2017**, 5, 8, 1600973.
2. 9-Gwinner, M. C.; Kabra, D.; Roberts, M.; Brenner, T. J. K.; Wallikewitz, B. H.; McNeill, C.; Friend, R. H.; Sirringhaus, H. **Highly Efficient Single-Layer Polymer Ambipolar Light-Emitting Field-Effect Transistor**s. *Adv. Mater.* **2012**, *24*, 2728–2734.
3. 23-Takenobu, T.; Bisri, S. Z.; Takahashi, T.; Yahiro, M.; Adachi, C.; Iwasa, Y. **High Current Density in Light-Emitting Transistors of Organic Single Crystals**. *Phy. Rev. Lett.* **2008**, *100*, 066601.
4. Ke, T.-H.,; Gehlhaar, R.; Chen, C.-H.; Lin, J.-T.; Wu, C.-C.; Adachi, C. **High Efficiency Blue Light Emitting Unipolar Transistor Incorporating Multifunctional Electrodes**. *App. Phys. Lett.* **2009**, *94*, 153307.
5. Nakanotani, H.; Kabe, R.; Yahiro, M.; Takenobu, T.; Iwasa, Y.; Adachi, C. **Blue-Light-Emitting Ambipolar Field-Effect Transistors Using an Organic Single Crystal of 1,4-Bis(4-methylstyryl)benzene**. *Appl. Phys. Express* **2008**, *1*, 091801.
6. Nakanotani, H.; Saito, M.; Nakamura, H.; Adachi, C. **Highly Balanced Ambipolar Mobilities with Intense Electroluminescence in Field-Effect Transistors based on Organic Single Crystal Oligo(p-Phenylenevinylene) Derivatives**. *Appl. Phys. Lett.* **2009**, 95, 033308.
7. 12- Tandy, K.: Ullah, M.; Burn, P. L.; Meredith, P.; Namdas; E. B. **Unlocking the full potential of light emitting field-effect transistors by engineering charge injection layers**. *Org. Electer.* **2013**, *14*, 2953-2961.